1-11-2013

Systems analysis of apoptosis protein expression allows the case-specific prediction of cell death responsiveness of melanoma cells.

Egle Passante
Royal College of Surgeons in Ireland

Maximilian L. Würstle
Royal College of Surgeons in Ireland

Christian T. Hellwig
Royal College of Surgeons in Ireland

Martin Leverkus
University of Heidelberg

Markus Rehm
Royal College of Surgeons in Ireland

Citation

Passante E, Wurstle ML, Hellwig CT, Leverkus M, Rehm M. Systems analysis of apoptosis protein expression allows the case-specific prediction of cell death responsiveness of melanoma cells. Cell Death and Differentiation. 2013;20:1521–1531.

Systems Analysis of Apoptosis Protein Expression allows the case-specific Prediction of Cell Death Responsiveness of Melanoma Cells

Running Title: Prediction of cell death responses in melanoma

Egle Passante[1,2,†], Maximilian L Würstle[1,2,†], Christian T Hellwig[1,2], Martin Leverkus[3], Markus Rehm[1,2,*]

[1]Department of Physiology & Medical Physics, [2]Centre for Systems Medicine, Royal College of Surgeons in Ireland, Dublin 2, Ireland; [3]Section of Molecular Dermatology, Department of Dermatology, Venereology, and Allergology, Medical Faculty Mannheim, University of Heidelberg, Germany. [†]These authors contributed equally.

* To whom correspondence should be addressed.
Dr. Markus Rehm
Department of Physiology and Medical Physics
Royal College of Surgeons in Ireland
RCSI York House, York Street
Dublin 2, Ireland

Phone: +353-1-402-8563
Fax: +353-1-402-2447
E-mail: mrehm@rcsi.ie

Abstract

Many cancer entities and their associated cell line models are highly heterogeneous in their responsiveness to apoptosis inducers and, despite a detailed understanding of the underlying signalling networks, cell death susceptibility currently cannot be predicted reliably from protein expression profiles. Here, we demonstrate that an integration of quantitative apoptosis protein expression data with pathway knowledge can predict the cell death responsiveness of melanoma cell lines. By a total of 612 measurements, we determined the absolute expression (nM) of 17 core apoptosis regulators in a panel of 11 melanoma cell lines, and enriched these data with systems-level information on apoptosis pathway topology. By applying multivariate statistical analysis and multi-dimensional pattern recognition algorithms, the responsiveness of individual cell lines to TRAIL or dacarbazine could be predicted with very high accuracy (91% and 82% correct predictions), and the most effective treatment option for individual cell lines could be pre-determined *in silico*. In contrast, cell death responsiveness was poorly predicted when not taking knowledge on protein-protein interactions into account (55% and 36% correct predictions). We also generated mathematical predictions on whether anti-apoptotic Bcl-2 family members or x-linked inhibitor of apoptosis protein (XIAP) can be targeted to enhance TRAIL responsiveness in individual cell lines. Subsequent experiments, making use of pharmacological Bcl-2/Bcl-xL inhibition or siRNA-based XIAP depletion, confirmed the accuracy of these predictions. We therefore demonstrate that cell death responsiveness to TRAIL or DTIC can be predicted reliably in a large number of melanoma cell lines when investigating expression patterns of apoptosis regulators in the context of their network-level interplay. The capacity to predict responsiveness at the cellular level may contribute to personalising anti-cancer treatments in the future.

Key Words: Systems biology; Cell Death; Apoptosis; Melanoma; Cancer; TRAIL.

Introduction

The past decades of molecular cancer research have demonstrated that many cancer entities, including malignant melanoma, are biologically highly heterogeneous. As a consequence of biological heterogeneity, only subsets of patient populations benefit from anti-cancer chemotherapies. For example, on average only 15% of metastatic melanoma patients respond to the standard single-agent chemotherapy based on the proapoptotic alcylating agent dacarbazine (DTIC) [1]. Likewise, alternative chemotherapeutics or combination treatments with DTIC so far did not result in more effective therapies [1]. Inter-individual heterogeneity is also thought to contribute considerably to the unsustainably high attrition rates of phase II/III clinical trials, since cohort recruitment is often not informed by tools that allow to predict whether patients are likely to respond to the treatment tested [2]. Biological heterogeneity in gene and protein expression has been captured in numerous biomarker discovery studies in order to identify, by statistical means, whether molecular signatures can predict drug responsiveness. However, these traditional approaches so far are rather unsuccessful, with most biomarker candidates failing at the clinical validation stage [3]. In melanoma, the presence of V600E-mutated B-Raf kinase is such a marker, and can be found in approximately 50% of patients with advanced disease. Whenever V600E-mutated B-Raf is found, the inhibitor Vemurafenib has proved to be a remarkable success as monotherapy [4]. The remaining patient population, however, still receives DTIC-based chemotherapy or immune therapy with ipilimumab, a CTLA-4 antagonizing antibody. Most recently combination therapies of programed death (PD) -1 receptor directed antibodies combined with ipilimumab showed a dramatic success, indicating that immune-mediated cell death is a successful way to control melanoma metastasis [5]. Even though deregulations in apoptosis signaling are known to limit melanoma responsiveness to various therapies [6], so far no apoptosis-related protein expression patterns could be firmly associated with DTIC

responsiveness or responsiveness to other apoptosis-inducing agents in patients or cell line model systems. A broader multi-parametric system-level approach towards cell death signaling in cell line models is therefore warranted and may contribute to informing future translational research strategies.

Apoptosis signals are transduced by two main pathways (extrinsic and intrinsic) which are tightly regulated by a complex interplay of multiple proteins [7-8]. Therefore, a large number of possibilities exist by which apoptosis signal transduction may be impaired. Integrating information on protein-protein interplay and pathway topology into data sets on protein expression amounts may therefore enhance the capacity of multivariate statistical models to accurately and case-specifically predict cell death responsiveness. The perspectives offered by systems biological and systems medical approaches [9], and the first successful proof-of-principle systems medical studies in the field of cancer and apoptosis [10-11] support this notion. Here, we therefore developed a system-level approach of knowledge- and data-driven multivariate statistical modeling and applied this to a panel of malignant human melanoma cell lines in order to identify whether baseline protein expression patterns carry information that indicate susceptibility to apoptosis inducing drugs. We were able to reliably predict the responsiveness of individual cell lines to known inducers of extrinsic or intrinsic apoptosis tumour necrosis factor-related apoptosis-inducing ligand (TRAIL) and DTIC, respectively. Predictions were sufficiently accurate to devise a decision tool that identifies the more efficient cell death inducer for individual cell lines. For poorly responding cell lines, we successfully validated further *in silico* predictions on which proteins need to be targeted by molecular perturbations in order to increase or restore responsiveness to TRAIL.

Results

Defining functional groups of apoptosis signalling proteins for a knowledge- and data-driven systems modelling approach.

Since decision points in apoptosis signal transduction are under the control of multi-protein interactions, we integrated basic pathway knowledge on protein-protein interplay into baseline expression data. This was achieved by defining functional groups, each of which comprised a limited number of proteins that were related to each other by simple arithmetic operations. These operations reflected the functional relationship of these proteins within the apoptosis signaling network that is initiated by tumour necrosis factor-related apoptosis-inducing ligand (TRAIL) (Fig.1A). In brief, the TRAIL pathway is induced by TRAIL binding to death receptors DR4 and DR5. DR4/5 then recruit the adapter protein FADD and form the death-inducing signaling complex (DISC). Caspase-8 is activated on the DISC, but caspase-8 activation can be antagonized by competitive binding of the catalytically inactive homologue cFLIP. Caspase-8 cleaves and activates the BH3-only protein Bid as well as effector caspase-3. Truncated Bid promotes the permeabilisation of the outer mitochondrial membrane by activating the pore-forming proteins Bax and Bak, and by inhibiting anti-apoptotic Bcl-2 family members Bcl-2, Bcl-xL and Mcl-1. Through Bax/Bak pores, cytochrome-c (cyt-c) and the XIAP antagonist Smac are released into the cytosol. Cyt-c activates Apaf-1, and Apaf-1 oligomerises to form the caspase-9-activating apoptosome complex. Caspase-9 proteolytically activates caspase-3, with the inhibitor XIAP suppressing caspase activity. Caspase-3 cleaves a large number of target proteins and is the central driver of rapid apoptosis execution and cell death [7-8]. The intrinsic apoptosis pathway, which is induced by various forms of intracellular stresses, feeds in at the level of BH3-only proteins other than Bid. These BH3-only proteins are transcriptionally induced, posttranslationally

activated or stabilized, and contribute as Bax/Bak activators and/or as Bcl-2/Bcl-xL/Mcl-1 antagonists. To code this pathway by functional groups, the rationale was to keep these groupings arithmetically simple (sums, products or ratios of a small number of proteins), biologically justifiable, and to incorporate the expression amount of each protein only once (Fig.1B). For example, we defined a functional group that represents the key anti-apoptotic Bcl-2 family members by pooling the absolute amounts (nM) of Bcl-2, Bcl-xL and Mcl-1. Likewise, we defined a functional group for the mitochondrial Bax/Bak pore formation capacity by pooling the amounts of Bax and Bak. By multiplying the amounts of Apaf-1 and caspase-9, we defined a functional group that represents the caspase-9-activating apoptosome complex. Here, the multiplication ensures that the value for this group approaches zero when either Apaf-1 or caspase-9 expression is very low or absent. With similar reasoning, we multiplied the pooled DR expression with the amount of FADD to represent the DISC. Functional groups of apoptotic caspases and their antagonists were defined as ratios (cFLIP/caspase-8 and XIAP/caspase-3). Following these groupings, the three remaining proteins (Bid, cyt-c, Smac) were kept as individual variables. While cyt-c is known to be an abundant protein [12], only a fraction of the cyt-c pool would be expected to contribute to apoptosis signaling. For example, significant amounts of cyt-c may be immobilized by cardiolipin interactions [13-14]. Likewise, the cyt-c redox status and additional molecular interactions in the cytosol following cyt-c release from the mitochondria are not captured in this study but may further modify the amount of cyt-c that contributes to apoptosome formation [15-17]. Such interactions could be merged in the cyt-c functional group in the future. Similarly, other proteins not quantified in this study that functionally overlap with Bid or Smac, such as other BH3-only proteins or Omi/HtrA2, could form functional groups with these in future extended quantification studies (i.e. a functional unit for BH3-only proteins and a functional unit for XIAP antagonists).

To parameterize the functional groups, we determined the expression profiles of these 17 key proteins involved in TRAIL-induced apoptosis signaling in a panel of 11 melanoma cell lines. With the exception of DR4 and DR5, whose cell surface expressions were determined by indirect immunofluorescence (Supplemental Fig.S1A), all protein amounts were measured by quantitative immunoblotting at 12 bit dynamic range (see methods for details; absolute protein concentrations are provided as Supplemental Table 1). Representative 8-bit converted immunoblotting signals are shown in Supplemental Fig.S1B. An overview of the relative protein expression within the melanoma cell line panel, based on 612 quantifications, is presented in Fig.1C and demonstrates high heterogeneity across the cell line panel.

Multi-dimensional pattern recognition identifies a relation between functional groups of apoptosis regulators and cell death responsiveness to TRAIL and DTIC.

As part of a data-driven modeling approach [18], we next applied a principle component analysis (PCA) [19-20] to the data set of the functional groups. This was followed by the integration of drug response data into the PCA output and a spatial segmentation of cell lines clusters with similar responsiveness by a pattern recognition approach. A step-by-step workflow of the modeling and analysis procedures is provided as Supplemental Figure 2 and can be consulted in parallel to the following results section.

A principal component analysis is a multivariate statistical procedure which reduces the dimensionality of complex multi-dimensional data sets by mathematical transformation into principle components. Slightly simplified, this transformation can be understood as a rotation of the data around their mean so that previously independent variables (the 9 dimensions of the functional groups; Fig.1B) now jointly define new axes. These new axes are the principal components (PCs) and describe the principal component space. While each PC consists of contributions by all variables that are found in the original data set, the contributions of these

variables differ for each PC according to specific weighting coefficients, as shown below. The PCA is geared towards representing as much of the data variance as possible in the first few PCs, thereby making the information content of the remaining PCs largely negligible for further analyses and allowing for a dimensionality reduction to a small number of PCs. We correspondingly could visualize this when showing the PCA results in a modified scree plot (Fig.2A). The first four principle components were required to reflect 85% of the data variance found in the functional groups, and these four principle components fulfilled the Kaiser criterion [21-22] (Fig.2A). The Kaiser criterion is a decision guideline which states that only PCs with an eigenvalue of one or above will need to be used for further analysis as this indicates that these PCs contain more information on data variance than a single variable in the original data set. The first four principle components were therefore retained for all subsequent analyses and procedures. The coefficients for the weightings of the functional groups in these PCs are displayed in Fig.2B, and the respective numerical values are provided as Supplemental Table 2. The coefficients indicated that the first principle component is strongly influenced by multiple functional groups: The anti-apoptotic Bcl-2 family members are antagonized by Bax+Bak. Similarly, contributions by the XIAP/caspase-3 ratio are antagonized by caspase-9*Apaf-1. (DR4+5)*FADD and Bid are strong contributors to the second principle component, as is cyt-c. The cFLIP/casp-8 ratio most prominently influenced the fourth principle component. We used the PCs to define a 4-dimensional Euclidean space into which we positioned the 11 melanoma cell lines according to the values of their functional groups. To this end, the numerical values of the functional groups were multiplied with the respective weighting coefficients in the PCs. Associated visualizations naturally had to be limited to the first three dimensions, which still reflect 71% of the original data variance (Fig2C). Cell lines with similar compositions of the functional groups would have been expected to cluster together. However, no obvious clusters could be detected. Rather, cell

lines were scattered throughout the PC space (Fig.2C), indicating a high variability in the values of the functional groups across the melanoma cell line panel.

We next investigated whether the spatial positions of the cell lines are related to their cell death responsiveness. To this end, we measured the overall cell death induced by TRAIL and by DTIC, the standard melanoma chemotherapeutic in B-Raf negative melanoma, in all cells lines. DTIC is a pro-drug that is converted intracellularly by mitochondrial cytochrome P450 to the alkylating agent MTIC, and induces apoptosis through the intrinsic pathway [23]. The cell death responses to TRAIL and also to DTIC were highly heterogeneous across the cell line panel, and individual cell lines typically also presented with different levels of responsiveness to TRAIL or DTIC (Fig.2D). Control measurements in presence of pan-caspase inhibitor zVAD-fmk in highly responsive cell lines demonstrated that cell death was executed primarily by apoptosis (Supplemental Fig.S3). The cell lines in the PC space were then color coded according to their TRAIL or DTIC responsiveness (Fig.2E,F). To this end, cell lines were defined as being resistant (0-10% cell death; black) or responsive (graded into "low" (10-30% cell death; red), "medium" (30-60% cell death; yellow) or "high" (>60% cell death; green)). Interestingly, cell lines with a similar TRAIL responsiveness appeared to occupy common regions in the 3D PC space (Fig.2E), and these response regions did not intersect when visually segmented (see also a 360° rotation provided as Supplemental Movie 1). Regions in the 3D PC space that reflect similar drug susceptibility were also found for DTIC treatments (Fig.2F). Also these response regions appeared to be separable by visual segmentation (best seen in the 360° rotation provided as Supplemental Movie 2 and in a view from an alternative angle provided as Supplemental Fig.S4). Corresponding to the cell line panel responding differently to TRAIL or DTIC, also the spatial regions that reflect similar levels of susceptibility differed between the TRAIL and DTIC (Fig.2E,F; Supplemental Movies 1,2). To determine whether the spatial regions that indicate different levels of drug

responsiveness could also be separated objectively, we applied a linear discriminant analysis (LDA) to the 4-dimensional PC space. A canonical LDA is a pattern recognition approach that mathematically defines linear functions with the aim to optimally separate multiple classes of objects in *n*-dimensional space [24]. The LDA working principle is visualised for a simplified 2D scenario in Fig.2G. LDA accurately separated the TRAIL response groups: All cell lines were correctly classified (Fig.2H). Likewise, a very good separation was achieved for DTIC, with 10 out of 11 cell lines correctly classified (91%) (Fig.2H).

Taken together, we found that spatial regions exist which represent distinct levels of drug responsiveness. These spatial regions differ between the drugs investigated, and for each drug these can be separated by an objective mathematical pattern recognition approach. Therefore, even though the cell lines are very heterogeneous in their protein expression profiles, these protein profiles, together with basic pathway knowledge, can be used to relate expression patterns to cell death susceptibility with high accuracy.

Case-specific predictions of TRAIL and DTIC responsiveness in malignant melanoma cell lines allow the *in silico* identification of optimal treatments.

To determine whether our approach has the capacity to predict cell death responsiveness case- and drug-specifically, we next applied "leave-one-out" cross-validations (LOOCV). To this end, 11 new PCAs were conducted to cover all possible combinations of 10 from the pool of melanoma cell lines. Clusters of common responsiveness in each PCA were then identified by LDA as described above. The missing cell lines (test cell lines) were positioned into the four dimensional PC spaces according to their functional group values, and their responsiveness was predicted based on the LDA-defined cluster associated with the PC space position. These predictions were validated against experimentally measured cell death susceptibility. Exemplary 2D projections of the 3D PC spaces for TRAIL responsiveness

demonstrate visually that test cell lines positioned in close proximity to cell lines that were of similar responsiveness (Fig.3A). The predictive power of this approach was very high for both TRAIL- and DTIC-responsiveness, with 10 and 9 cell lines being positioned in the correct LDA-defined response regions (91% and 82% prediction accuracy, respectively) (Fig.3B). As a control, we performed the same procedure on the raw protein expression data rather than the functional groups data. The accuracy dropped significantly, with the responsiveness of only 55% and 36% of the cell lines correctly predicted for TRAIL or DTIC treatments, respectively. This highlights that accurate predictions can only be made when taking pathway knowledge into account.

We next investigated whether this predictive capacity is sufficiently high to case-specifically determine the optimal treatment *in silico*. "Optimal treatment" here is defined as the drug that evokes the higher amount of cell death, with either drug being an acceptable choice if both treatments were predicted to induce comparable amounts of cell death. In contrast, wrong predictions would suggest treatments that in experiments induce lower amounts of cell death than the alternative treatment option. Cell line-specific treatment suggestions were correct for 10 out of the 11 cell lines (Fig.4). Only for PM-WK cells the better treatment option was not identified. These results indicate that our approach is very powerful in accurately predicting drug responsiveness and in exploiting this as a decision tool to select the optimal treatment option between TRAIL and DTIC for individual cell lines.

Knowledge- and data-driven systems modeling can predict targeted perturbations that sensitize poorly responding melanoma cell lines to TRAIL.

The positioning of each cell line in the PC space is coded by the values calculated for their functional groups. We therefore hypothesized that this information could also be exploited to generate case-specific predictions on how to sensitize poor TRAIL responders by targeted

drugs or by siRNA-based protein depletion. As a representative targeted drug, we used ABT-737, a well characterized synthetic antagonist of the anti-apoptotic Bcl-2 family members Bcl-2 and Bcl-xL [25] that is currently also tested in clinical trials as a sensitizer of melanoma to proliferation inhibitors such as MEK inhibitors [26]. To generate predictions on which poorly responding cell line can be sensitized by ABT-737, we determined how the position of individual cell lines in the PC space would change upon elimination of Bcl-2 and Bcl-xL. The vector for the direction of this repositioning can be calculated from the PCA results by moving in opposite direction to the coefficients of the targeted functional group in all PC axes (Fig.5A). The distance by which individual cell lines are repositioned then depends on the combined amounts of its targets (Bcl-2+Bcl-xL) (Fig.5B). The resulting repositioning vectors were applied to four representative cell lines that poorly respond to TRAIL (RPM-EP, RPM-MC, MeWo, Preyer). For the TRAIL-resistant MeWo and Preyer cells, the vectors pointed in the direction of cell lines that are moderately TRAIL sensitive (yellow) (Fig.5C), indicating that addition of ABT-737 may enhance TRAIL responsiveness. In contrast, for the poor TRAIL responders RPM-EP or RPM-MC the vectors did not result in a movement towards regions of higher TRAIL responsiveness (Fig.5C). The predictions on high vs. low sensitization by ABT-737 for these four cell lines were validated experimentally. As predicted, ABT-737 strongly sensitized MeWo and Preyer cells to TRAIL, whereas sensitization of RPM-EP and RPM-MC was far less pronounced (Fig.5D). Control experiments ensured that ABT-737 readily entered all cell lines and was capable to sensitize these for mitochondrial translocation of ectopically expressed YFP-Bax (Supplemental Fig.5). We next applied the same approach to a scenario of siRNA-mediated XIAP depletion. Our calculations on movement direction and movement distance (Fig.5E,F) suggested that out of four poor TRAIL responders (Preyer, MeWo, RPM-EP, MM-AN) only MM-AN could be relocated closer to cell lines with higher TRAIL responsiveness (Fig.5G). Again, these

predictions were confirmed by subsequent experiments. Even though XIAP was efficiently depleted, as confirmed by immunoblotting (Fig.5H), using a previously validated siRNA sequence [27-28], only MM-AN cells were significantly sensitized to TRAIL (Fig.5H). These results therefore demonstrate that accurate predictions can be made on which proteins should be targeted to efficiently enhance cellular responsiveness of individual cell lines that poorly respond to TRAIL.

Discussion

The elimination of cancer cells by cell death induction is a mainstay of anti-cancer chemotherapies [29] and is likely an important predictor if treatment modalities such as immune therapy can be effective to control disease relapse. Apoptotic cell death is an irreversible cell fate decision, and is regulated by the complex interplay of multiple proteins that control signal transduction during the initiation and execution phases of programmed cell death. Here, we integrated quantitative information on systems-level protein interplay with multivariate statistical analysis and pattern recognition algorithms in order to generate predictions on the susceptibility of melanoma cell lines to TRAIL and DTIC (Fig.6). These predictions were highly accurate (91% and 82% correct predictions) and outperformed the predictive capacity of a systems knowledge-independent statistical analysis (55% and 36% prediction accuracy). Our findings indicate that to reliably predict cell death responsiveness the multi-factorial control of apoptosis signaling needs to be taken into account, and that this can be achieved by integrating systems-level pathway knowledge into the analysis of protein expression patterns.

Our knowledge- and data-driven modeling approach was successfully applied for drug treatments that are known to induce extrinsic and intrinsic apoptosis, and controls with caspase inhibitor zVAD-fmk in selected responsive cell lines demonstrated that apoptosis was the primary cell death modality (Supplemental Fig.S3). Performance scores were very high for TRAIL-induced cell death, which may be attributable to our quantitative measurements having covered all critical TRAIL signal transducers. Furthermore, TRAIL-induced apoptosis can proceed independent of protein neosynthesis, explaining why a systems analysis of baseline protein expression is sufficient to accurately predict TRAIL responsiveness. Since TRAIL ligands are currently investigated in clinical trials and since improved 2nd generation ligands are currently in preclinical development [30-31], our systems

approach may provide possibilities to identify TRAIL-responsive melanoma by molecular profiling, and by extension may assist in patient stratification as part of future clinical trial designs. We were also able to predict DTIC-induced cell death, albeit with slightly lower accuracy. The induction of apoptosis by genotoxic stress is mediated by p53-dependent transcriptional induction of BH3-only proteins such as Noxa, Puma and Bik [32-33]. Baseline expression amounts of these BH3-only proteins are typically very low, and p53 is rarely mutated in melanoma (<5%) [34]. This may explain why we achieved predictive capacity for DTIC treatments as well, even though we did not measure BH3-only protein amounts other than Bid. However, Bid has been reported to also contribute to genotoxic apoptosis [35], and in this context is cleaved by death receptor-independent, presumably ripoptosome-activated caspase-8 [36-37]. A more comprehensive profiling of BH3-only proteins may nevertheless further enhance the performance scores, and including information on the p53 mutational status will be required when further developing this approach for cancer entities in which p53 is more frequently mutated. Likewise, molecular coverage of alternative cell death mechanisms, such as necroptosis signaling, may further improve the performance of our approach since in our measurements we captured total cell death rather than only specific apoptotic cell death. Such an expansion could therefore be particularly important at conditions where apoptosis-independent cell death signaling plays a substantial role [38-39].

Various previous studies suggested that abundance measurements of proteins which regulate apoptosis in melanoma, including anti-apoptotic Bcl-2 family members and XIAP [40-41], may be sufficient to predict cell death susceptibility. Our study instead demonstrates that apoptosis susceptibility depends on the quantitative interplay of multiple proteins, and that targeted interventions to enhance apoptosis responsiveness need to be identified on a case-by-case basis. Our study also highlights that due to the heterogeneity in apoptosis protein expression a single optimal treatment strategy cannot be suggested for a given tumor entity, as exemplified

by malignant melanoma. Since we have investigated a large number of proteins (n=17) in a large panel of cell lines (n=11) by quantitative measurements, the biological heterogeneity in apoptosis protein expression and cell death responsiveness in melanoma model systems may have been more representatively captured in our study than was the case in previous reports. Importantly, despite the heterogeneity in protein expression, our systems-level data analysis allowed us to obtain insight into both drug responsiveness and resistance mechanisms of individual cell lines. Together, these findings may have important implications for future translational biomarker identification strategies in the field of melanoma and other highly heterogeneous cancers. Since the classical repertoire of preclinical and clinical statistical biomarker screening so far yielded surprisingly few biomarkers that successfully translated into clinical practice [3], integrating systems level information and data analysis approaches may contribute to improving this situation in the future.

It can be speculated that our approach could be used to analyze primary tumors or metastases for their capacity to execute apoptosis, to predict therapy responsiveness, and to generate personalized treatment recommendations. However, a validation for clinical application at the present time is challenging due to the need for large scale, quantitative protein expression analysis. Commonly used tissue immunohistochemistry in clinical diagnostics, based on immunoperoxidase staining, is of limited dynamic range, and stained tissue slides are typically not calibrated for quantitative readouts. Sufficient fresh frozen tissue as required for quantitative immunoblotting is rarely collected or available, and reverse phase protein arrays, which can be applied for large-scale multi-sample protein quantification in clinical specimens [42], require the prior identification or development of high quality antibodies for each protein of interest. A successful clinical implementation of pathway-based systems models will furthermore necessitate the integration with mathematical models that cover higher level aspects that are known to critically influence therapy responsiveness and outcome. These

include for example models reflecting drug pharmacokinetics and pharmacodynamics, tumor vascularization, and information on the tumor microenvironment and immune infiltration. Higher scale modeling strategies that can make use of such information have been described in recent years [10, 43] and have the potential to be linked to systems models that have been validated *in cellulo*. Likewise, models that capture cell survival due to treatment-induced changes in protein expression profiles[44] would be valuable tools that in the future could be combined with our approach and that may serve to better predict chemotherapy efficacy. Our study may therefore make an important contribution towards developing systems-based predictive tools that can be applied in a clinical context in the future.

Experimental Procedures

Materials: Dacarbazine (DTIC) was purchased from Sigma-Aldrich Ireland Ltd (Dublin, Ireland), ABT-737 was from Biorbyt (Riverside, UK), Mitotracker Red was from Invitrogen (UK). Human recombinant TRAIL was a generous gift from Carlos Ricardo Rodrigues dos Reis, University of Groningen.

Cell Culture and Drug Treatments: The human melanoma cell lines PM-WK, RPM-MC, RPM-EP, MM-RU, MM-AN, and MM-LH were generously provided by Randy H. Byers (Boston University School of Medicine, Department of Dermatology) and cultured as previously described [45]. The following human melanoma cells were obtained either from ATCC or DSMZ (Deutsche Sammlung von Mikroorganismen und Zellkulturen GmbH) and cultured as described: A375 (ATCC CRL-1619), MeWo (ATCC HTB-65), SK-Mel-30 (SK-Mel; ACC 151), and IGR-37 (IGR; ACC 237). Preyer melanoma cells (generated from a subcutaneous melanoma metastasis) were kindly provided by A. Schwaaf and E.B. Bröcker, University of Würzburg, Germany). All melanoma cell lines were cultured in DMEM (Lonza, Slough, UK) supplemented with 4 mM L-glutamine, 4.5 g/l glucose, 10% (w/v) heat-inactivated fetal bovine serum (Sigma-Aldrich), 100 U/ml penicillin and 100 µg/ml streptomycin (Sigma-Aldrich) as published [46]. Cells were grown at 5% CO_2 and 37°C. For cell death analysis, cells were incubated for 24 h with TRAIL (100 ng/ml) or for 48 h with DTIC (1 mg/ml).

Transfections: siRNA known to specifically silence the expression of XIAP and non-silencing control sequences were obtained by Sigma-Aldrich (XIAP: AAG UGG UAG UCC UGU UUC AGC [28]; control: UUC UCC GAA CGU GUC ACG U[dT]). Cells were

transfected with siRNA (100 nM) in Optimem with Lipofectamine 2000 (Invitrogen, Paisley, UK) according to the manufacturer's instruction at least 24 h prior to drug treatment. Protein depletion was validated by immunoblotting. Transient transfections for the expression of YFP-Bax were conducted as described before [47] and cell were analyzed by conventional widefield fluorescence microscopy.

Immunoblotting and Densitometry: Cells were harvested, washed in PBS and homogenised in lysis buffer (62.5 mM Tris-HCl, pH 6.8, 10% (v/v) glycerin, 2% (w/v) SDS, 1 mM phenylmethylsulfonyl fluoride, 1 μg/ml leupeptin and 5 g/ml aprotinin). Lysates were heated to 95°C for 15 min and cleared of debris by centrifugation. Protein content was assayed using the Micro BCA protein assay kit (Thermo Scientific, Dublin, Ireland). Samples (20 μg) were resolved on 10-15% SDS-polyacrylamide gels (150 V for approximately 1 h). Proteins were transferred to nitrocellulose membranes (Whatman, Kent, UK) in transfer buffer (25 mM Tris, 192 mM glycine, 20% methanol (v/v) and 0.01 (w/v) SDS) at 18 V for 1.5 h. Membranes were blocked in 5% nonfat dry milk in distilled water at room temperature for 1 h and incubated with primary antibodies overnight at 4°C. Membranes were then washed with TBST three times for 5 min and incubated with anti-mouse, anti-rabbit or anti-goat peroxidase-conjugated secondary antibodies (Millipore, Molsheim, France). The following primary antibodies were used: a rabbit polyclonal APAF-1 antibody (No. 559683, BD Transduction Laboratories, San Jose, CA, USA), a rabbit polyclonal Bak antibody (sc-832, Santa Cruz Biotechnology), a rabbit polyclonal Bax antibody (No. Q07815, Millipore), a mouse monoclonal Bcl-2 antibody (sc-509, Santa Cruz Biotechnology), a mouse monoclonal Bcl-X_L antibody (sc-8392, Santa Cruz Biotechnology), a goat polyclonal Bid antibody (AF860, R&D Systems), a rabbit polyclonal caspase-3 antibody (#9662, Cell Signaling Technology, Danvers, MA, USA), a mouse monoclonal caspase-8 antibody (No 804-242,

Alexis, San Diego, CA, USA), a rabbit polyclonal caspase-9 antibody (No. 218794, Calbiochem /Merck Bioscience, Nottingham, UK), a mouse monoclonal cytochrome-c antibody (No. 556433, BD Transduction Laboratories), a mouse monoclonal DR4 antibody (ab47138, AbCam), a rabbit polyclonal DR5 antibody (No 804-298, Alexis San Diego, CA, USA), a mouse monoclonal FADD antibody (No. 610399, BD Transduction Laboratories), a mouse monoclonal FLIP antibody (No 804-428, Alexis), a mouse monoclonal Mcl-1 antibody ((No. 559027, BD Transduction Laboratories), a rabbit polyclonal SMAC/Diablo antibody (AF789, R&D Systems), a mouse monoclonal XIAP antibody (No 610763, BD Transduction Laboratories), a mouse monoclonal β-actin antibody (A5441, Sigma-Aldrich). Anti-mouse IgG, anti-goat IgG, anti-rabbit IgG peroxidase conjugated secondary antibodies (AP124P, AP106P, AP132P, Millipore) were used at a dilution of 1:5000 for 1 h. Blots were washed and developed using the Immobilon™ western chemiluminescence HRP substrate (Millipore). Chemiluminescence was detected at a depth of 12-bit in the linear detection range of a Fuji LAS 4000 CCD system (Fujifilm UK Ltd., Bedfordshire, UK). Special care was taken not to overexpose in order to guarantee accurate quantifications. For all proteins at least three independent membranes were analysed. Densitometry was performed on 12-bit raw images using ImageJ 1.4.1o software (National Institute of Health, USA, http://rsb.info.nih.gov/ij) [48]. For each protein, the integrated density of the signal was measured, corrected for background signals and adjusted to loading controls. Intensities were then compared to signals obtained from HeLa cell extracts run on the same gels. Absolute protein levels in HeLa cells (nM) have been determined by us and others before by comparison to titrated purified proteins [48]; Lindner et al., 2012). For visual presentation, 12-bit images were contrast adjusted and converted to 8-bit.

Flow cytometry: Flow cytometry was performed on a BD LSRII flow cytometer (BD Bioscience, Oxford, UK) equipped with a high throughput system (HTS) to acquire samples directly from 96 well plates. DR-4 and DR-5 surface expression was assessed by indirect immunofluorescence. Briefly, cells were harvested, washed, fixed in 4% paraformaldehyde in PBS for 15 min and incubated with a mouse monoclonal DR4 (AbCam) or DR5 antibody (Alexis) (5 μg/10^6 cells) for 30 min followed by secondary anti-mouse FITC-conjugated antibody (AbCam) (1:50 dilution) for 30 min in the dark. Controls were stained with secondary antibody only. After each incubation, cells were washed with 3% BSA in PBS to remove excess antibody. FITC was excited at 488 nm and fluorescence emission was collected through a 552/50 nm band-pass filter and a 505 nm long pass filter. The relative expression of death receptors was determined by comparison of specific staining intensities. For cell death measurements, cells were detached and incubated on an orbital shaker (300 rpm) with propidium iodide (2 μg/ml) (Sigma-Aldrich) at room temperature for 15 min in the dark. Propidium iodide was excited with a 561 nm laser line and fluorescence emission was collected through a 605/40 nm band-pass filter and a 570 nm long pass filter. Data were analysed using Cyflogic software (CyFlo Ltd, Turku, Finland). Cell death measurements were conducted as endpoint readings. Control experiments in selected high and low responding cell lines were performed at multiple time points with AnnexinV-FITC (Biovision, CA)/propidium iodide co-staining to ensure the absence of significant amounts of early apoptotic cells (Annexin V+/PI-) at the time of measurement.

Data processing and analysis for knowledge- and data-driven modeling: All data processing and analysis was performed using a programming code developed for MATLAB 2007b (The Mathworks, UK), equipped with the statistics toolbox. Protein data in functional groups were rescaled prior to statistical analysis by dividing through the respective standard

deviation, followed by mean centering. A principal component analysis (PCA) based on the correlation matrix of these data was performed [19-20]. The Kaiser criterion and an adapted scree plot were used to identify how many principal components needed to be retained for subsequent analyses [21-22]. For visualizations, scatter plots were generated from the first three principle components. Cell lines were assigned to classes of cell death responsiveness using k-means clustering. Linear Discriminant Analysis [24] was performed in the first four principle components to determine the quality of response class separation in the PC space. To determine predictive capacity, leave-one-out cross-validation (LOOCV) was applied iteratively on training sets of 10 cell lines, with the remaining cell line being the test set. The test cell line was placed into the PC space according to its specific functional group values and associated PC coefficients calculated from the training cell lines. LDA was applied to determine whether the test cell line positioned in the spatial region that corresponded to its drug responsiveness. To predict the consequences of targeted protein perturbations, the target protein concentrations were set to zero, and the displacement of individual cell lines was calculated by multiplying the changes in the respective functional groups with the coefficients in the first three PCs. Movement towards spatial regions of higher responsiveness were considered to be predictive of sensitization.

Statistical Testing: Student's *t*-tests were used to identify statistically significant differences between treatment groups. *p*-values above 0.05 were considered not to be significant. *p*-value ranges below 0.05 were indicated in the respective figure panels. Analyses were performed using SPSS 15 (Lead Technologies Inc.).

References

1. Lui P, Cashin R, Machado M, Hemels M, Corey-Lisle PK, Einarson TR. Treatments for metastatic melanoma: synthesis of evidence from randomized trials. *Cancer treatment reviews* 2007; **33**(8)**:** 665-80.

2. Paul SM, Mytelka DS, Dunwiddie CT, Persinger CC, Munos BH, Lindborg SR *et al.* How to improve R&D productivity: the pharmaceutical industry's grand challenge. *Nat Rev Drug Discov* 2010; **9**(3)**:** 203-14.

3. Poste G. Bring on the biomarkers. *Nature* 2011; **469**(7329)**:** 156-7.

4. Chapman PB, Hauschild A, Robert C, Haanen JB, Ascierto P, Larkin J *et al.* Improved survival with vemurafenib in melanoma with BRAF V600E mutation. *N Engl J Med* 2011; **364**(26)**:** 2507-16.

5. Wolchok JD, Kluger H, Callahan MK, Postow MA, Rizvi NA, Lesokhin AM *et al.* Nivolumab plus Ipilimumab in Advanced Melanoma. *N Engl J Med* 2013.

6. Soengas MS, Lowe SW. Apoptosis and melanoma chemoresistance. *Oncogene* 2003; **22**(20)**:** 3138-51.

7. Hellwig CT, Passante E, Rehm M. The molecular machinery regulating apoptosis signal transduction and its implication in human physiology and pathophysiologies. *Curr Mol Med* 2011; **11**(1)**:** 31-47.

8. Taylor RC, Cullen SP, Martin SJ. Apoptosis: controlled demolition at the cellular level. *Nat Rev Mol Cell Biol* 2008; **9**(3)**:** 231-41.

9. Auffray C, Chen Z, Hood L. Systems medicine: the future of medical genomics and healthcare. *Genome Med* 2009; **1**(1)**:** 2.

10. Gorelik B, Ziv I, Shohat R, Wick M, Hankins WD, Sidransky D *et al.* Efficacy of weekly docetaxel and bevacizumab in mesenchymal chondrosarcoma: a new theranostic method combining xenografted biopsies with a mathematical model. *Cancer Res* 2008; **68**(21)**:** 9033-40.

11. Hector S, Rehm M, Schmid J, Kehoe J, McCawley N, Dicker P *et al.* Clinical application of a systems model of apoptosis execution for the prediction of colorectal cancer therapy responses and personalisation of therapy. *Gut* 2012; **61**(5)**:** 725-33.

12. Waterhouse NJ, Goldstein JC, von Ahsen O, Schuler M, Newmeyer DD, Green DR. Cytochrome c maintains mitochondrial transmembrane potential and ATP generation after outer mitochondrial membrane permeabilization during the apoptotic process. *J Cell Biol* 2001; **153**(2)**:** 319-28.

13. Quinn PJ, Dawson RM. Interactions of cytochrome c and [14C]-carboxymethylated cytochrome c with monolayers of phosphatidylcholine, phosphatidic acid and cardiolipin. *Biochem J* 1969; **115**(1)**:** 65-75.

14. Ott M, Zhivotovsky B, Orrenius S. Role of cardiolipin in cytochrome c release from mitochondria. *Cell Death Differ* 2007; **14**(7)**:** 1243-7.

15. Chandra D, Bratton SB, Person MD, Tian Y, Martin AG, Ayres M *et al.* Intracellular nucleotides act as critical prosurvival factors by binding to cytochrome C and inhibiting apoptosome. *Cell* 2006; **125**(7)**:** 1333-46.

16. Mei Y, Yong J, Liu H, Shi Y, Meinkoth J, Dreyfuss G *et al.* tRNA binds to cytochrome c and inhibits caspase activation. *Mol Cell* 2010; **37**(5)**:** 668-78.

17. Vaughn AE, Deshmukh M. Glucose metabolism inhibits apoptosis in neurons and cancer cells by redox inactivation of cytochrome c. *Nat Cell Biol* 2008; **10**(12)**:** 1477-83.

18. Janes KA, Yaffe MB. Data-driven modelling of signal-transduction networks. *Nat Rev Mol Cell Biol* 2006; **7**(11)**:** 820-8.

19. Hotelling H. Analysis of a complex of statistical variables into principal components. *J. Educ. Psych.* 1933; **24**.

20. Pearson K. On lines and planes of closest fit to systems of points in space. *Philosophical Magazine* 1901; **2**(6)**:** 599-572.

21. Kaiser HF. The Application of Electronic Computers to Factor Analysis. *Educational and Psychological Measurement* 1960; **20**(1)**:** 141-151.

22. Cattell RB. The Scree Test For The Number Of Factors. *Multivariate Behavioral Research* 1966; **1**(2)**:** 245-276.

23. Reid JM, Kuffel MJ, Miller JK, Rios R, Ames MM. Metabolic activation of dacarbazine by human cytochromes P450: the role of CYP1A1, CYP1A2, and CYP2E1. *Clin Cancer Res* 1999; **5**(8)**:** 2192-7.

24. Fisher RA. THE USE OF MULTIPLE MEASUREMENTS IN TAXONOMIC PROBLEMS. *Annals of human genetics* 1936; **7**(2)**:** 179-188.

25. Oltersdorf T, Elmore SW, Shoemaker AR, Armstrong RC, Augeri DJ, Belli BA *et al.* An inhibitor of Bcl-2 family proteins induces regression of solid tumours. *Nature* 2005; **435**(7042)**:** 677-81.

26. Cragg MS, Jansen ES, Cook M, Harris C, Strasser A, Scott CL. Treatment of B-RAF mutant human tumor cells with a MEK inhibitor requires Bim and is enhanced by a BH3 mimetic. *The Journal of clinical investigation* 2008; **118**(11)**:** 3651-9.

27. Laussmann MA, Passante E, Dussmann H, Rauen JA, Wurstle ML, Delgado ME *et al.* Proteasome inhibition can induce an autophagy-dependent apical activation of caspase-8. *Cell Death Differ* 2011; **18**(10)**:** 1584-97.

28. Wilkinson JC, Cepero E, Boise LH, Duckett CS. Upstream regulatory role for XIAP in receptor-mediated apoptosis. *Mol Cell Biol* 2004; **24**(16)**:** 7003-14.

29. Hanahan D, Weinberg RA. Hallmarks of cancer: the next generation. *Cell* 2011; **144**(5)**:** 646-74.

30. Hellwig CT, Rehm M. TRAIL signaling and synergy mechanisms used in TRAIL-based combination therapies. *Mol Cancer Ther* 2012; **11**(1)**:** 3-13.

31. Wilson NS, Yang B, Yang A, Loeser S, Marsters S, Lawrence D *et al.* An Fcgamma receptor-dependent mechanism drives antibody-mediated target-receptor signaling in cancer cells. *Cancer Cell* 2011; **19**(1)**:** 101-13.

32. Weber A, Kirejczyk Z, Potthoff S, Ploner C, Hacker G. Endogenous Noxa Determines the Strong Proapoptotic Synergism of the BH3-Mimetic ABT-737 with Chemotherapeutic Agents in Human Melanoma Cells. *Translational oncology* 2009; **2**(2)**:** 73-83.

33. Cory S, Adams JM. The Bcl2 family: regulators of the cellular life-or-death switch. *Nat Rev Cancer* 2002; **2**(9)**:** 647-56.

34. Lubbe J, Reichel M, Burg G, Kleihues P. Absence of p53 gene mutations in cutaneous melanoma. *J Invest Dermatol* 1994; **102**(5)**:** 819-21.

35. Kohler B, Anguissola S, Concannon CG, Rehm M, Kogel D, Prehn JH. Bid participates in genotoxic drug-induced apoptosis of HeLa cells and is essential for death receptor ligands' apoptotic and synergistic effects. *PLoS ONE* 2008; **3**(7)**:** e2844.

36. Tenev T, Bianchi K, Darding M, Broemer M, Langlais C, Wallberg F *et al.* The Ripoptosome, a Signaling Platform that Assembles in Response to Genotoxic Stress and Loss of IAPs. *Mol Cell* 2011.

37. Feoktistova M, Geserick P, Kellert B, Dimitrova DP, Langlais C, Hupe M *et al.* cIAPs Block Ripoptosome Formation, a RIP1/Caspase-8 Containing Intracellular Cell Death Complex Differentially Regulated by cFLIP Isoforms. *Mol Cell* 2011.

38. Kreuzaler P, Watson CJ. Killing a cancer: what are the alternatives? *Nat Rev Cancer* 2012.

39. Vanlangenakker N, Vanden Berghe T, Vandenabeele P. Many stimuli pull the necrotic trigger, an overview. *Cell Death Differ* 2012; **19**(1)**:** 75-86.

40. Tang L, Tron VA, Reed JC, Mah KJ, Krajewska M, Li G *et al.* Expression of apoptosis regulators in cutaneous malignant melanoma. *Clin Cancer Res* 1998; **4**(8)**:** 1865-71.

41. Hiscutt EL, Hill DS, Martin S, Kerr R, Harbottle A, Birch-Machin M *et al.* Targeting X-linked inhibitor of apoptosis protein to increase the efficacy of endoplasmic reticulum stress-induced apoptosis for melanoma therapy. *J Invest Dermatol* 2010; **130**(9)**:** 2250-8.

42. Mueller C, Liotta LA, Espina V. Reverse phase protein microarrays advance to use in clinical trials. *Molecular oncology* 2010; **4**(6)**:** 461-81.

43. Eissing T, Kuepfer L, Becker C, Block M, Coboeken K, Gaub T *et al.* A computational systems biology software platform for multiscale modeling and simulation: integrating whole-body physiology, disease biology, and molecular reaction networks. *Front Physiol* 2011; **2:** 4.

44. Laussmann MA, Passante E, Hellwig CT, Tomiczek B, Flanagan L, Prehn JH *et al.* Proteasome Inhibition Can Impair Caspase-8 Activation upon Submaximal Stimulation of Apoptotic Tumor Necrosis Factor-related Apoptosis Inducing Ligand (TRAIL) Signaling. *J Biol Chem* 2012; **287**(18)**:** 14402-11.

45. Byers HR, Etoh T, Doherty JR, Sober AJ, Mihm MC, Jr. Cell migration and actin organization in cultured human primary, recurrent cutaneous and metastatic melanoma. Time-lapse and image analysis. *The American journal of pathology* 1991; **139**(2)**:** 423-35.

46. Geserick P, Drewniok C, Hupe M, Haas TL, Diessenbacher P, Sprick MR *et al.* Suppression of cFLIP is sufficient to sensitize human melanoma cells to TRAIL- and CD95L-mediated apoptosis. *Oncogene* 2008; **27**(22)**:** 3211-20.

47. Dussmann H, Rehm M, Concannon CG, Anguissola S, Wurstle M, Kacmar S *et al.* Single-cell quantification of Bax activation and mathematical modelling suggest pore formation on minimal mitochondrial Bax accumulation. *Cell Death Differ* 2010; **17**(2)**:** 278-90.

48. Rehm M, Huber HJ, Dussmann H, Prehn JH. Systems analysis of effector caspase activation and its control by X-linked inhibitor of apoptosis protein. *Embo J* 2006; **25**(18)**:** 4338-49.

Acknowledgements: The authors wish to thank Carlos Ricardo Rodrigues dos Reis, University of Groningen, for providing human recombinant TRAIL and Frank A Lincoln for technical assistance. This research was supported by grants from the Health Research Board Ireland (RP/2008/7), and the National Biophotonics and Imaging Platform (HEA PRTLI Cycle 4), and the EU Framework Programme 7 (APO-DECIDE). The work in the laboratory of M. L. is supported by grants from the DFG (Le 953/6-1 and 8-1), the Wilhelm-Sander-Stiftung (2008.072.1), and the Mildred-Scheel-Stiftung (Projekt 109891).

Conflict of interest: The authors declare no financial conflicts of interest.

Figure Legends

Fig.1: Coding and parameterising functional groups of apoptosis signal proteins for knowledge- and data-driven systems modelling.

(A) Pathway diagram of extrinsic apoptosis signal transduction through the TRAIL pathway. **(B)** Combination of apoptosis signalling proteins into functional groups by simple arithmetic operations. **(C)** Relative levels of protein expression within the melanoma cell line panel. Circles summarize 612 quantifications and circle sizes are proportional to the protein quantities determined from n=3 independent detections each. Green and red indicate anti- and pro-apoptotic proteins, respectively. Absolute protein amounts are provided as Supplemental Table 1.

Fig.2: Functional groups of apoptosis regulators highlight an association between protein expression profiles and cell death responsiveness to TRAIL and DTIC.

(A) A Principal component analysis (PCA) was applied to the functional groups of the melanoma cell line panel, and results are shown as a scree plot. Bar graphs show the contribution of each principal component (PC) towards explaining the data variance. Eigenvalues of PCs fulfilling the Kaiser criterion are shaded in grey. **(B)** Bar graphs show the coefficients for all functional groups in the first four PCs. Coefficient values are provided as Supplemental Table 2. **(C)** Graphical illustration of the distribution of melanoma cell lines along the first three PCs. Circle sizes decrease with distance from the observer to aid 3D visualization. **(D)** Cell death in response to TRAIL or DTIC. Cells were treated for 48 h and cell death was measured by propidium iodide uptake. Data are means + s.d. above untreated controls and were pooled from n=3 independent repeat experiments. **(E,F)** Cell lines in the 3D PC space were color coded according to cell death responsiveness to TRAIL or DTIC,

respectively. Color codes reflect resistance (black), low responsiveness (red), or medium responsiveness (yellow). Cell lines with high responsiveness (green) were not detected. 3D rotations are available as Supplementary Movies 1 and 2. **(G)** Linear Discriminant Analysis (LDA) was applied to the 4-dimensional PC space. The 2D schematic visualizes the principle of separating response regions by this pattern recognition approach. **(H)** The performance of the response group separation in the 4-dimensional space by LDA is shown by listing the amounts of correctly classified cell lines.

Fig.3: Systems analysis generates highly accurate case-specific predictions on TRAIL and DTIC responsiveness of melanoma cell lines.

(A) Determination of predictive power by leave-one-out cross-validation (LOOCV). 2D projections of 3D PC spaces calculated from combinations of 10 cell lines are shown. LDA was applied to define spatial regions for resistant cell lines, low and medium responders for TRAIL treatment. Circle sizes decrease with distance, thereby representing the third PC dimension. Test cell lines (open circles, highlighted by arrows) were placed into the respective PC spaces according to their functional group values. If test cell lines positioned in spatial regions that were defined by prior LDA to correspond to their drug responsiveness, their responsiveness was considered to be predicted correctly. **(B)** Performance scores for correctly predicting drug responsiveness of test cell lines to TRAIL or DTIC by LOOCV-PCA and LDA in 4-dimensional space.

Fig.4: Case-specific predictions on TRAIL and DTIC responsiveness allow the *in silico* identification of optimal treatment options.

The predictive capacity of the systems approach was exploited as a treatment decision tool. Treatment recommendations were made *in silico* according to highest predicted

responsiveness to DTIC or TRAIL, respectively. Predictions were validated against experimental data. Predictions were labeled as correct (green) when the best treatment option could be identified, prediction were labeled as wrong (red) when the possibility existed that the better treatment option could be missed.

Fig.5: Prediction and experimental validation of targeted perturbations that sensitize poorly responding cell lines to TRAIL.

(A-D) Targeted perturbation with Bcl-2/Bcl-xL antagonist ABT-737. **(A)** Inverse vectorial addition of the coefficients of the Bcl-2+Bcl-xL+Mcl-1 functional group in the first 3 PCs. The resultant vector is shown in red and indicates the direction of cell line displacement in the PC space upon antagonizing this functional group by ABT-737. **(B)** Bar graphs show the distance by which individual cell lines are displaced in the 3D PC space when neutralizing Bcl-2 and Bcl-xL by ABT-737. **(C)** Combination of movement direction and distance shown in the 3D PC space for four poorly TRAIL-responsive cell lines. **(D)** Experimental validation of sensitization predictions. Cells were treated with 100 ng/ml TRAIL and/or 5 μM ABT-737 as indicated. Data show cell death above untreated controls (means + s.d. from n=3 independent experiments). Student's *t*-test was used for statistical analysis. **(E-H)** Targeted perturbation by siRNA-mediated XIAP depletion. **(E)** The red vector indicates the direction of cell line displacement by XIAP depletion. **(F)** Bar graphs indicate the distance of movement of individual cell lines in the 3D PC space upon eliminating XIAP. **(G)** Combination of movement direction and distance shown in the 3D PC space for four poorly TRAIL-responsive cell lines. **(H)** Experimental validation of sensitization predictions. Cells were treated with 100 ng/ml TRAIL 24 h after transfection with 100 nM XIAP siRNA or scrambled control siRNA. Data show cell death above controls transfected with scrambled

siRNA (means + s.d. from n=3 independent experiments). Student's *t*-test was used for statistical analysis. Immunoblot inserts show the efficacy of XIAP depletion by siRNA.

Fig.6: Workflow and associated functionalities for data- and knowledge-driven systems modeling to predict apoptosis sensitivity and treatment options.

The systems analysis of apoptosis protein expression allowed *(i)* to predict responsiveness of melanoma cell lines to TRAIL and DTIC, *(ii)* to predict optimal treatment options for individual cell lines, and *(iii)* to successfully identify targeted interventions that increased apoptosis responsiveness in treatment-resistant cells.

Figure 1

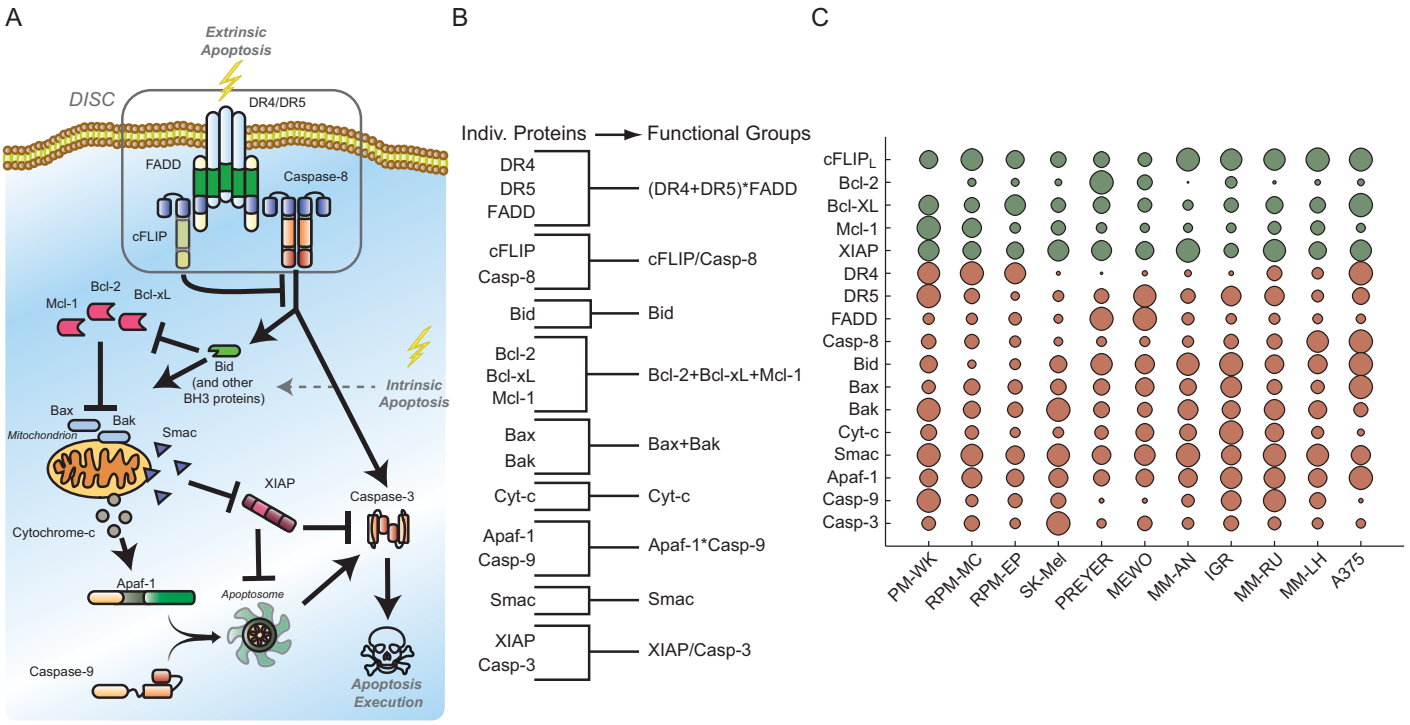
A
Extrinsic Apoptosis
DISC
DR4/DR5
FADD
Caspase-8
cFLIP
Bcl-2
Bcl-xL
Mcl-1
Bid (and other BH3 proteins)
Intrinsic Apoptosis
Bax
Bak
Mitochondrion
Smac
XIAP
Caspase-3
Cytochrome-c
Apaf-1
Apoptosome
Caspase-9
Apoptosis Execution
B
Indiv. Proteins
Functional Groups
DR4
DR5
FADD
(DR4+DR5)*FADD
cFLIP
Casp-8
cFLIP/Casp-8
Bid
Bid
Bcl-2
Bcl-xL
Mcl-1
Bcl-2+Bcl-xL+Mcl-1
Bax
Bak
Bax+Bak
Cyt-c
Cyt-c
Apaf-1
Casp-9
Apaf-1*Casp-9
Smac
Smac
XIAP
Casp-3
XIAP/Casp-3
C
cFLIPL
Bcl-2
Bcl-XL
Mcl-1
XIAP
DR4
DR5
FADD
Casp-8
Bid
Bax
Bak
Cyt-c
Smac
Apaf-1
Casp-9
Casp-3
PM-WK
RPM-MC
RPM-EP
SK-Mel
PREYER
MEWO
MM-AN
IGR
MM-RU
MM-LH
A375

Figure 2

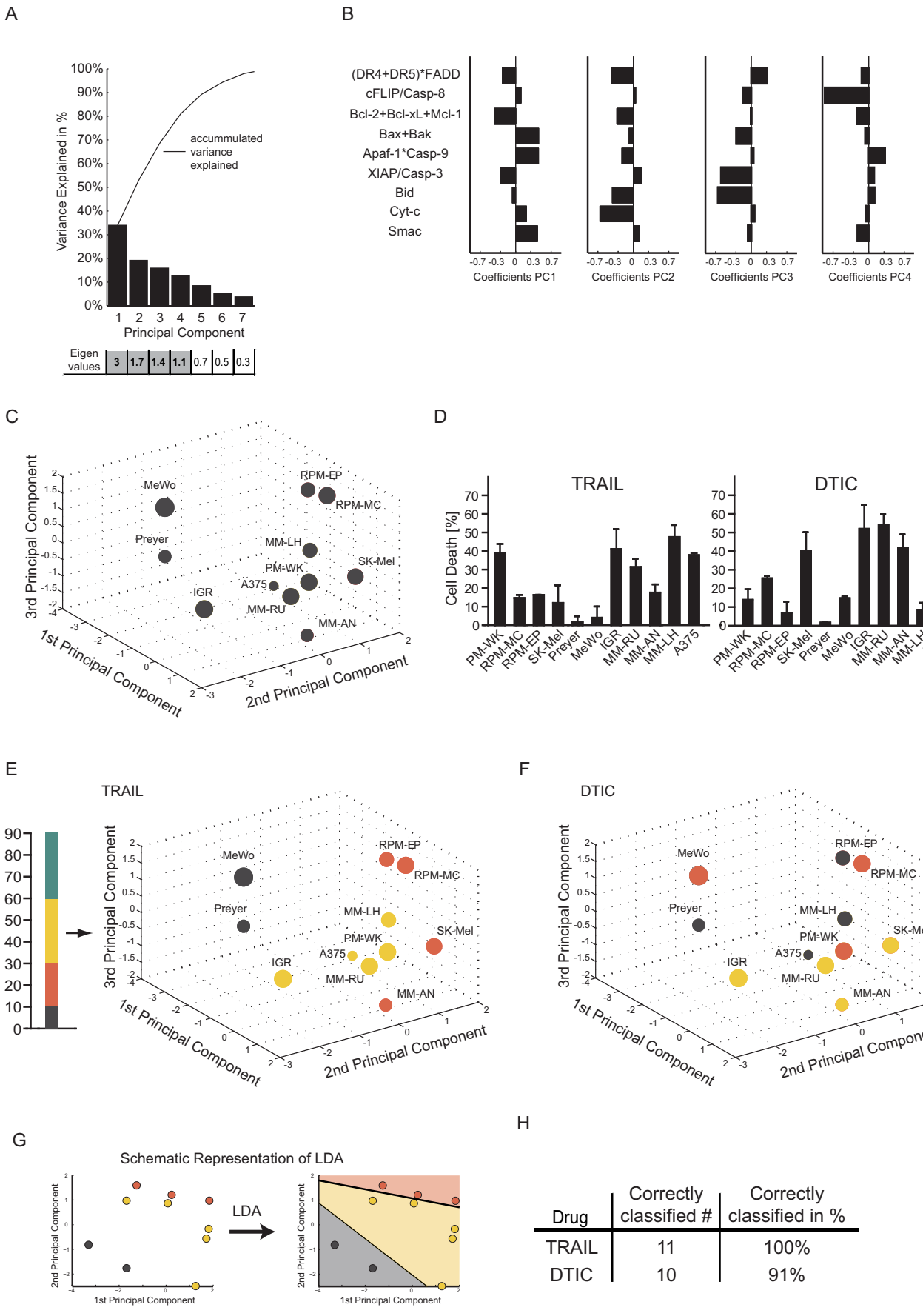
A
B
C
D
E
F
G
H
Variance Explained in %
accummulated variance explained
Principal Component
Eigen values
3
1.7
1.4
1.1
0.7
0.5
0.3
(DR4+DR5)*FADD
cFLIP/Casp-8
Bcl-2+Bcl-xL+Mcl-1
Bax+Bak
Apaf-1*Casp-9
XIAP/Casp-3
Bid
Cyt-c
Smac
Coefficients PC1
Coefficients PC2
Coefficients PC3
Coefficients PC4
3rd Principal Component
1st Principal Component
2nd Principal Component
MeWo
RPM-EP
RPM-MC
Preyer
MM-LH
PM-WK
SK-Mel
A375
IGR
MM-RU
MM-AN
TRAIL
DTIC
Cell Death [%]
PM-WK
RPM-MC
RPM-EP
SK-Mel
Preyer
MeWo
IGR
MM-RU
MM-AN
MM-LH
A375
Schematic Representation of LDA
LDA
Drug
Correctly classified #
Correctly classified in %
TRAIL
11
100%
DTIC
10
91%

Figure 3

A

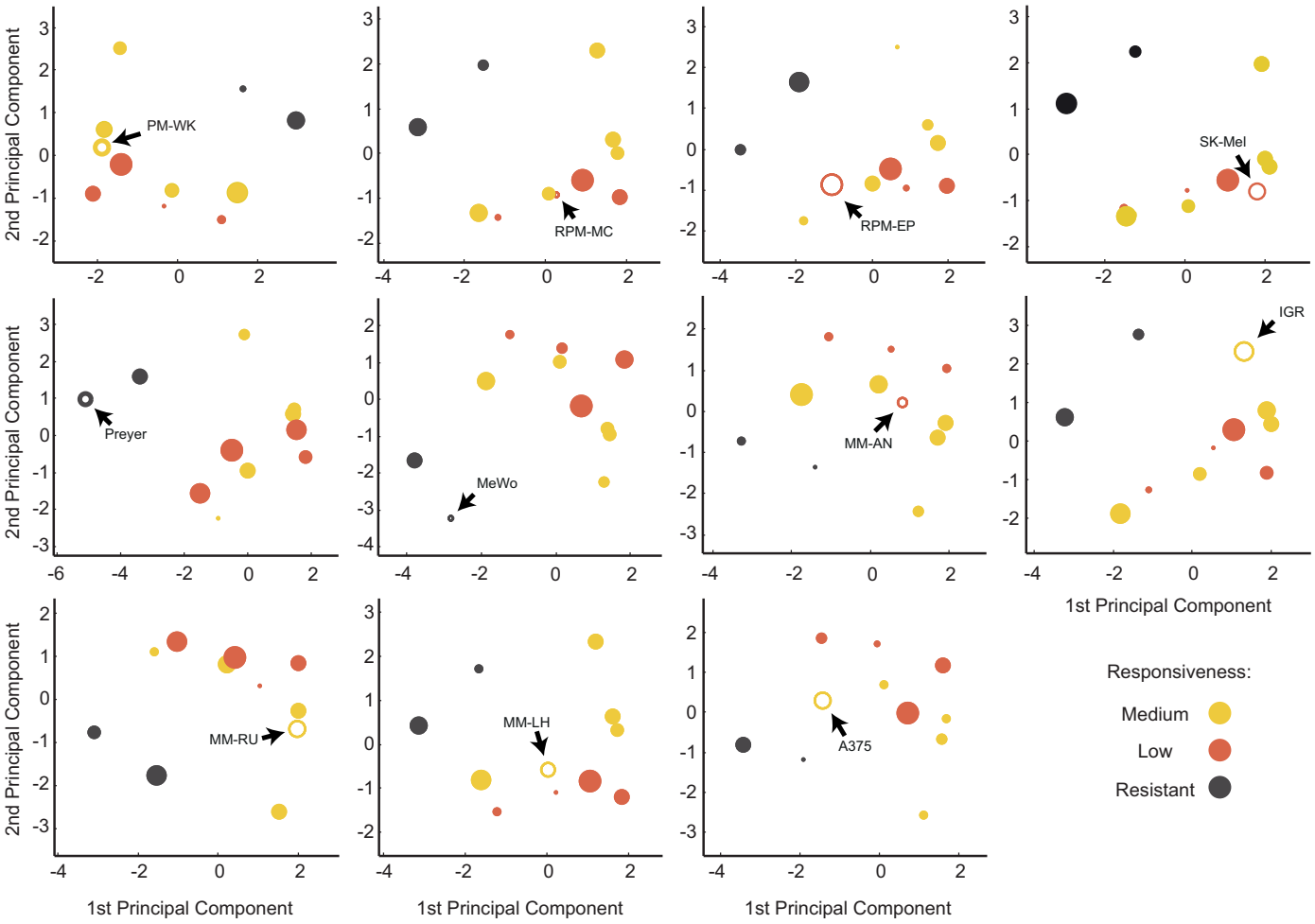

B Leave-one-out cross-validation:

Drug	Correctly predicted #	Correctly predicted in %
TRAIL	10	91%
DTIC	9	82%

Figure 4

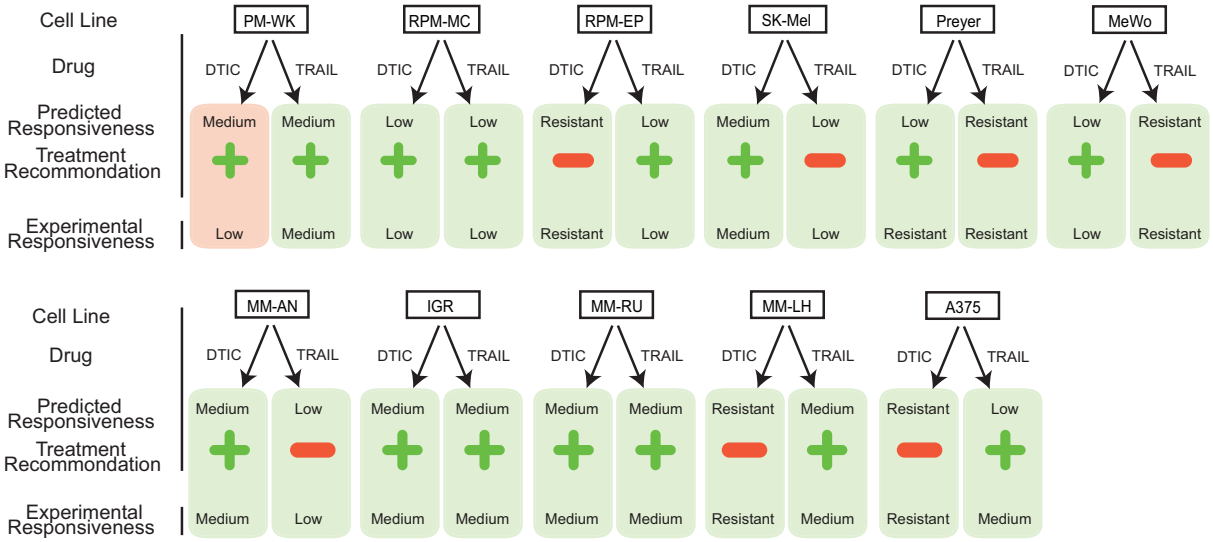
Cell Line
Drug
Predicted Responsiveness
Treatment Recommendation
Experimental Responsiveness
PM-WK
RPM-MC
RPM-EP
SK-Mel
Preyer
MeWo
DTIC
TRAIL
Medium
Low
Resistant
MM-AN
IGR
MM-RU
MM-LH
A375

Figure 5

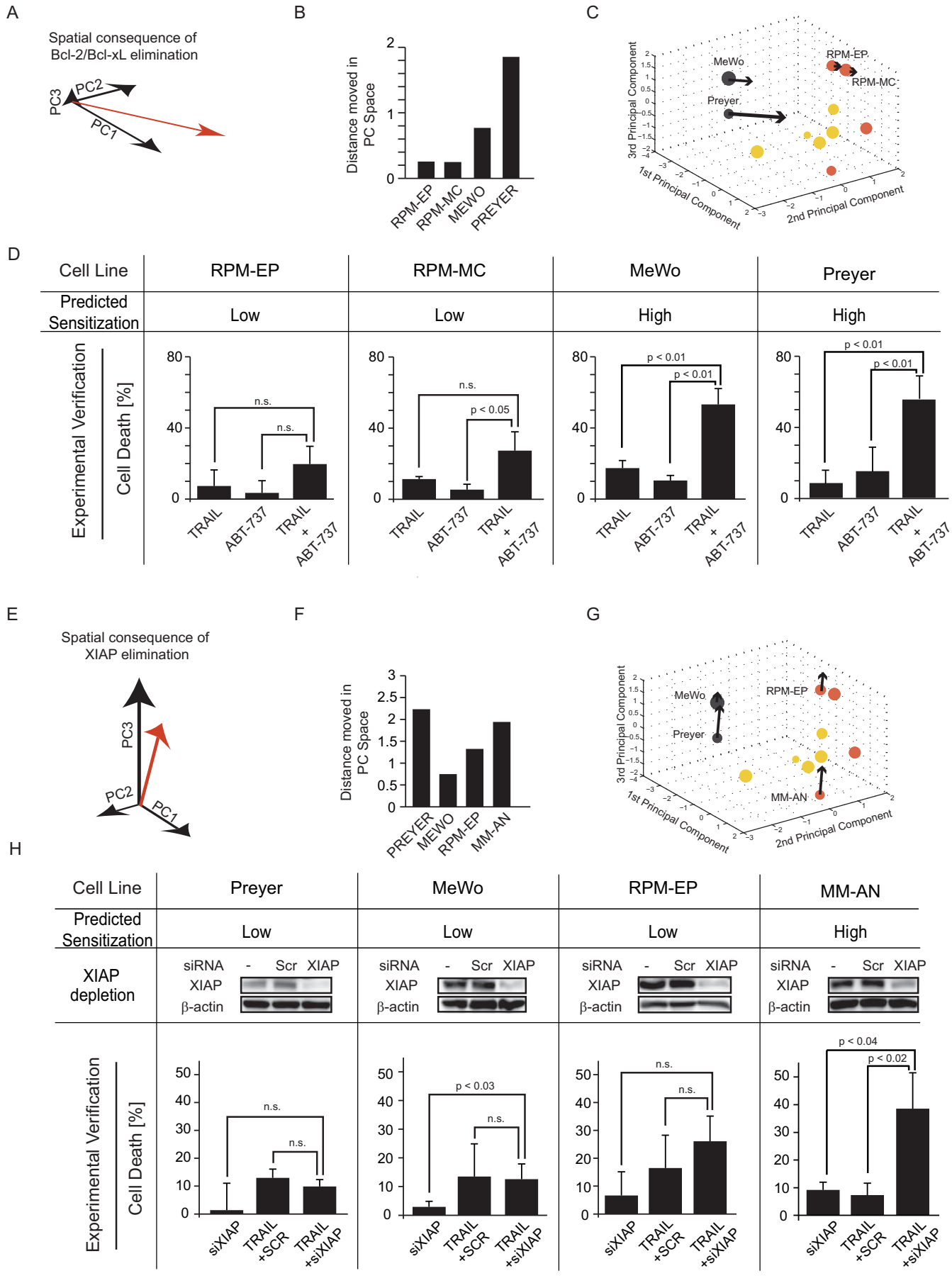
A
Spatial consequence of Bcl-2/Bcl-xL elimination
PC3
PC2
PC1
B
Distance moved in PC Space
RPM-EP
RPM-MC
MEWO
PREYER
C
MeWo
RPM-EP
RPM-MC
Preyer
3rd Principal Component
1st Principal Component
2nd Principal Component
D
Cell Line
RPM-EP
RPM-MC
MeWo
Preyer
Predicted Sensitization
Low
Low
High
High
Experimental Verification
Cell Death [%]
n.s.
p < 0.05
p < 0.01
TRAIL
ABT-737
TRAIL + ABT-737
E
Spatial consequence of XIAP elimination
PC3
PC2
PC1
F
Distance moved in PC Space
PREYER
MEWO
RPM-EP
MM-AN
G
MeWo
RPM-EP
Preyer
MM-AN
3rd Principal Component
1st Principal Component
2nd Principal Component
H
Cell Line
Preyer
MeWo
RPM-EP
MM-AN
Predicted Sensitization
Low
Low
Low
High
XIAP depletion
siRNA - Scr XIAP
XIAP
β-actin
Experimental Verification
Cell Death [%]
n.s.
p < 0.03
p < 0.04
p < 0.02
siXIAP
TRAIL +SCR
TRAIL +siXIAP

Figure 6

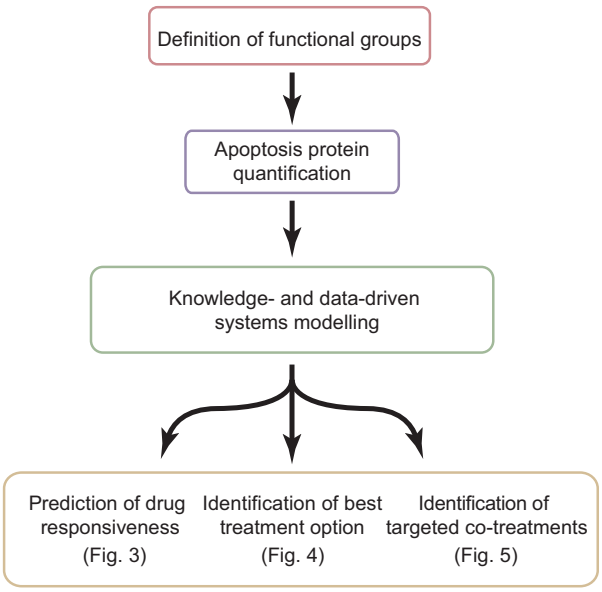
Definition of functional groups
Apoptosis protein quantification
Knowledge- and data-driven systems modelling
Prediction of drug responsiveness (Fig. 3)
Identification of best treatment option (Fig. 4)
Identification of targeted co-treatments (Fig. 5)